Journal of Power Sources 202 (2012) 78–84

Contents lists available at SciVerse ScienceDirect

Journal of Power Sources

journal homepage: www.elsevier.com/locate/jpowsour

Effect of strontium (Sr) doping on the conductivity of ceria

Nandini Jaiswal, Nitish Kumar Singh, Devendra Kumar, Om Parkash*

Department of Ceramic Engineering, Institute of Technology, Banaras Hindu University, Varanasi 221005, India

ARTICLE INFO

Article history:
Received 2 September 2011
Received in revised form 21 October 2011
Accepted 26 October 2011
Available online 18 November 2011

Keywords:
Doped ceria
Combustion synthesis
Impedance analysis
Electrical conductivity

ABSTRACT

A few compositions in the system $Ce_{1-x}Sr_xO_{2-x}$ with $0.05 \le x \le 0.20$ have been prepared by auto-combustion method. More than 93% of theoretical density has been achieved by sintering at 1350 °C for 4 h. Solid solution has formed in the composition with $x = 0.05$. All other compositions have been found to contain XRD lines of $SrCeO_3$ beside the major fluorite phase. Complex plane impedance analysis has clearly revealed the contribution of grains, grain boundaries, and electrode specimen interface to the total observed resistance of the sample. Conduction occurs mainly due to diffusion of O^{2-} ions through oxygen vacancies as indicated by values of activation energy of conduction. Composition, $Ce_{0.95}Sr_{0.05}O_{1.95}$ exhibits the highest ionic conductivity 3.26×10^{-3} S cm^{-1} at 500 °C among the series. Ionic conductivity decreases gradually with increasing x. This is due to the formation of a second phase $SrCeO_3$ and increasing probability of formation of neutral associated defect pairs, $Sr''_{Ce} - V_O^{\bullet\bullet}$.

1. Introduction

Solid oxide fuel cells (SOFCs) are the best promising candidates for a new generation power system due to their high efficiency, high waste-heat utilization, and greater fuel flexibility [1]. At present, SOFCs use yttria stabilized zirconia (YSZ) as solid electrolyte. YSZ exhibits sufficient oxygen ion conductivity around ~1000 °C. This high-temperature operation has several disadvantages. High operating temperature requires high cost materials for long term operation. Development of low-cost materials with high durability at cell operating temperatures is the key challenge facing this technology. Major challenges for the commercialization of SOFC, is to lower the temperature of operation using new more cost-effective solid electrolytes which exhibit high oxide ion conductivity in the temperature range 500–700 °C. The materials having potential for this purpose are based on ceria doped with divalent or trivalent cations [2–8]. Cells operating suitably in the temperature range 500–700 °C are termed as intermediate temperature solid oxide fuel cell (IT-SOFC). Ceria doped with Gd^{3+}(GDC) or Sm^{3+}(SDC) showed highest conductivity [9,10]. But Gd and Sm are very costly. A series of cations in the oxide form, such as CaO [11,12], SrO [13,14] have been investigated as dopants for CeO_2. It is reported that alkaline earth oxides are soluble in ceria up to a certain concentration resulting in formation of oxygen vacancies and enhance ionic conductivity.

In the present work, electrical conductivity of a series of strontium doped ceria has been investigated. Citrate–nitrate auto-combustion synthesis technique has been used to obtain nanocrystalline powders in the system $Ce_{1-x}Sr_xO_{2-x}$ with $0.05 \le x \le 0.20$. These materials have been characterised by measuring density and studying their microstructure using scanning electron microscope (SEM). Impedance analysis has been used to study their conduction behaviour. Compositions with $x = 0.05$, 0.1, 0.15, and 0.20 are designated as CSO5, CSO10, CSO15 and CSO20, respectively in the text.

2. Experimental

Powders were prepared using citrate–nitrate auto combustion technique. Ceric ammonium nitrate $(NH_4)_2[Ce(NO_3)_6]$, strontium nitrate $Sr(NO_3)_2$, and citric acid ($C_6H_8O_7 \cdot H_2O$) having purity greater than 99.5% were used as starting materials. Citric acid solution was added to mixed solution of ceric ammonium nitrate and strontium nitrate so that citrate to nitrate ratio of 0.3 was attained. This ratio was chosen based on the previous reports in the literature for combustion. The solution was evaporated at 200 °C on a hot plate till it became a gel. The gel was heated until it turned into a brown viscous mass. On further heating this burnt. The method uses the energy produced by the exothermic decomposition of a redox mixture of metal nitrates with an organic compound. In the combustion mixture, nitrates and citric acid behave as oxidants and fuels respectively. Pale yellowish ash was obtained after combustion.

The ash was calcined at 600 °C. The calcined powder was pressed into pellets by applying 70 kN load into a cylindrical shape (diameter ~15 mm and thickness ~1–2 mm). Finally, the pellets were

* Corresponding author. Tel.: +91 542 6701791; fax: +91 542 2368428.
E-mail address: oprakash.cer@itbhu.ac.in (O. Parkash).

0378-7753/$ – see front matter © 2011 Elsevier B.V. All rights reserved.
doi:10.1016/j.jpowsour.2011.10.140

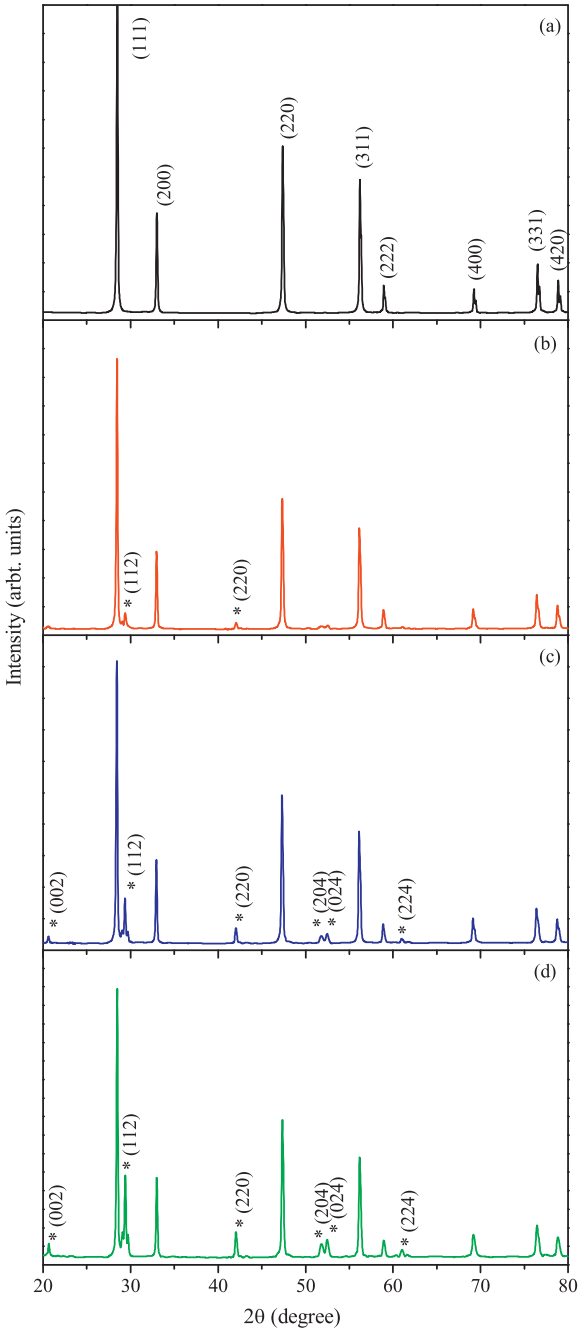

Fig. 1. Powder X-ray diffraction patterns of various compositions (a) CSO5, (b) CSO10, (c) CSO15 and (d) CSO20 sintered at 1350 °C.

sintered at 1350 °C for 4 h and cooled to room temperature. Density of the sintered samples was measured using Archimedes principle.

Powder X-ray diffraction patterns were recorded using a Rigaku high resolution powder X-ray diffractometer employing Cu $K_{\alpha 1}$ radiation and Ni-filter. Data were collected in the 2θ range from 20 to 80°. Lattice parameter was calculated using nonlinear least square fitting program 'UNITCELL' [15]. The reflection from (1 1 1) plane was used for the determination of the average crystallite size. The average crystallite size, D, of the prepared powder has been calculated from the Scherrer's formula:

$$D = \frac{0.9\lambda}{\beta \cos\theta} \quad (1)$$

where λ is the wavelength of the X-rays, θ is the diffraction angle and β is corrected full width at half maxima of the diffraction peak.

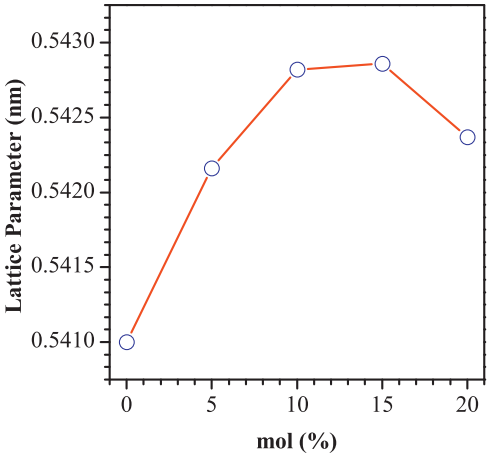

Fig. 2. Variation of lattice parameter as function of the dopant concentration for the system $Ce_{1-x}Sr_x O_{2-x}$.

Sintered pellets were polished using emery papers of grade 1/0, 2/0, 3/0, and 4/0 (Sia, Switzerland) followed by polishing on a velvet cloth with diamond paste of grade1/4-OS-475 (HIFIN). Then these were etched thermally at 1250 °C. Micrographs were taken with the help of scanning electron microscope (INSPECT 50 FEI').

Sintered pellets were polished on both sides and electroded with silver paint (fired at 700 °C for 15 min) for electrical measurements. Electrical conductivity of the silver coated pellets has been measured in the temperature range 200–500 °C at an interval of 25 °C using a Novocontrol Alpha-A High Performance Frequency Analyzer in the frequency range 1 Hz to 1 MHz with 1 V applied ac signal. Impedance analysis has been used to separate contribution of grains, grain boundaries and electrode–electrolyte interface to the total electrical resistance.

3. Results and discussion

Crystal phase and solubility of the dopants have been determined by XRD. Fig. 1 shows XRD patterns of CSO5, CSO10, CSO15 and CSO20 sintered powders. XRD patterns for the calcined powders are similar to those obtained after sintering except that the diffraction lines become sharper. This is due to grain growth occurring during sintering. Diffraction patterns were indexed on the basis of fluorite structure similar to CeO_2 using JCPDS file no. 43-1002 and perovskite type structure of $SrCeO_3$ using JCPDS file no. 47-1689. From these figures, it is clear that there is precipitation of second perovskite phase $SrCeO_3$ in addition to the fluorite phase for compositions with $x > 0.05$ in the present work. The lattice parameter is shown in Table 1. Change in lattice parameter is due to larger ionic radius of Sr^{2+} (1.26 Å) as compared to Ce^{4+} (0.97 Å) [16]. Lattice parameter of Sr^{2+}-doped ceria samples is plotted as a function of mol% as shown in Fig. 2.

Lattice parameter increases very rapidly with increasing SrO content up to 5 mol% and then slowly up to 10 mol%. It decreases

Table 1
Crystallite size, lattice parameter and % theoretical density of compositions of the system $Ce_{1-x}Sr_xO_{2-x}$.

S. n.	Compositions	Crystallite size of sintered powder (nm)	Lattice parameter (Å)	% of theoretical density
1.	$Ce_{0.95}Sr_{0.05}O_{1.95}$	55	5.421	96.8
2.	$Ce_{0.90}Sr_{0.1}O_{1.90}$	53	5.429	94.5
3.	$Ce_{0.85}Sr_{0.15}O_{1.85}$	54	5.429	93.0
4.	$Ce_{0.80}Sr_{0.2}O_{1.80}$	51	5.426	98.2

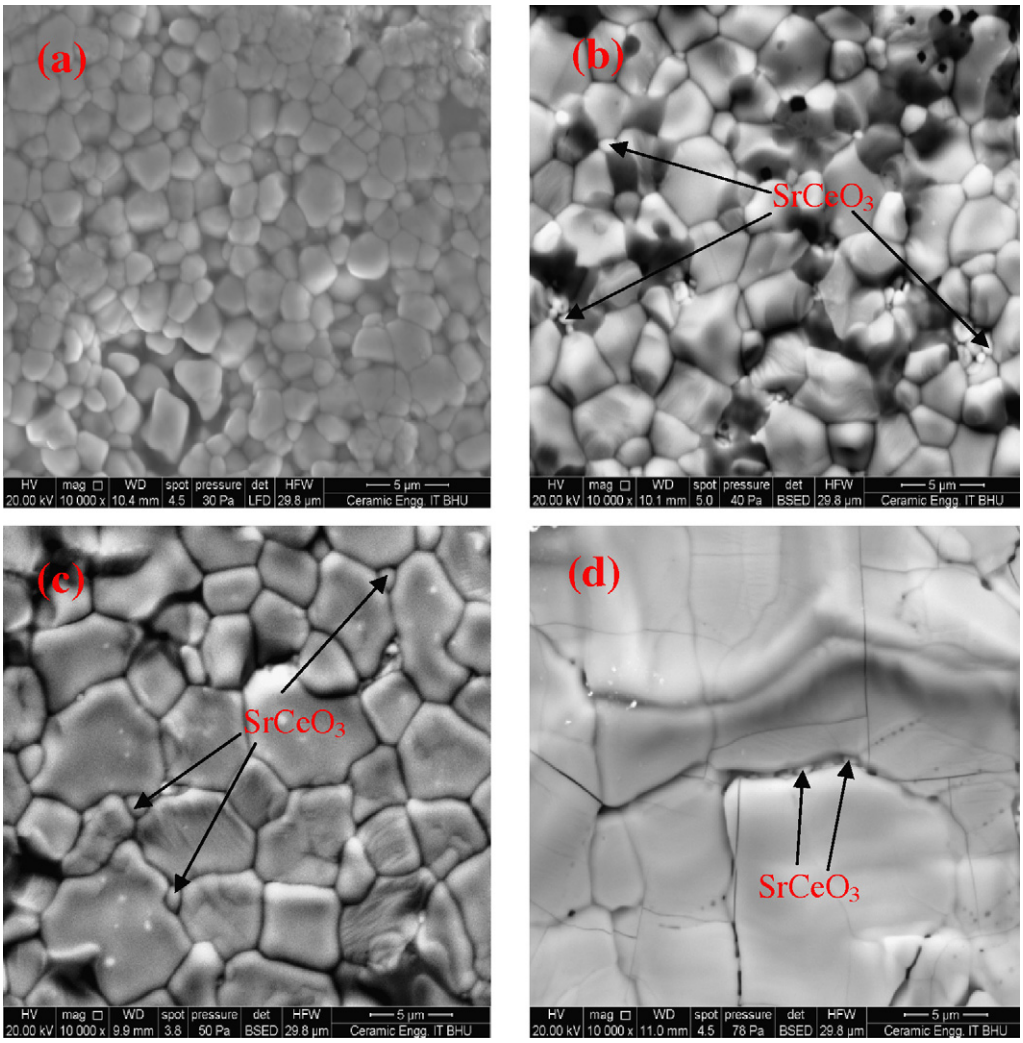

Fig. 3. Scanning electron micrograph of various compositions (a) CSO5, (b) CSO10, (c) CSO15 and (d) CSO20 etched at 1250 °C.

beyond 15 mol%. This shows that solid solubility of SrO in CeO_2 is between 5 and 10 mol%. This is in conformity with results of powder XRD (Fig. 1) which clearly show presence of the second perovskite, $SrCeO_3$ phase. Average crystallite size, D, of powders, calculated by Scherrer's formula from the XRD data was between 51 and 56 nm (Table 1). Pellets sintered at 1350 °C have densities more than 93% of the theoretical values (Table 1).

Fig. 3(a)–(d) shows SEM of thermally etched samples sintered at 1350 °C. It is noted that there is formation of dense material. Average grain size of compositions CSO5, CSO10, CSO15 and CSO20 determined by linear intercept method is approx. 2.6, 4.9, 5.1 and 13.1 μm respectively. Composition with $x = 0.05$ have spherical grains. Faceting is observed clearly in the compositions with $x > 0.05$. Presence of a second phase $SrCeO_3$ is also observed which has been indicated by arrows in the micrographs. This is in confirmity with results of XRD.

Electrical conductivity of the samples was studied using complex plane impedance analysis. Typical complex plane impedance plots of CSO5 and CSO10 at different temperatures are shown in Figs. 4(a)–(f) and 5(a)–(f) respectively. Impedance plots of all the compositions at 200 °C are shown in Fig. 6(a)–(d). Behaviour of CSO15 and CSO20 is essentially similar. At 200 °C, contribution of the grains and grain boundaries is clearly seen. With increasing temperature, relaxation frequency of all the polarization processes increases. This shifts the plots to right hand side. Arc corresponding to contribution of electrode polarization starts appearing at 250 °C. On the otherhand, the arc corresponding to contribution of grains disappears at 325 °C. It is noted from Fig. 6 that total resistance given by $R_g + R_{gb}$ is minimum for CSO5 among all the compositions. In order to see clearly, the contribution of the grains, the data is plotted on an expanded scale in the insets. Values of grains (R_g) and grain boundaries (R_{gb}) resistance can be determined from the

Table 2
Total conductivity (at 500 °C and 600 °C), activation energy of grains (E_g), grain boundaries (E_{gb}) and total (E_t) conductivity of various compositions of the system $Ce_{1-x}Sr_xO_{2-x}$.

S. n.	Compositions	σ_t at 500 °C (S cm^{-1})	σ_t at 600 °C (S cm^{-1})[a]	E_g (eV)	E_{gb} (eV)	E_t (eV)
1.	$Ce_{0.95}Sr_{0.05}O_{1.95}$	3.26×10^{-3}	1.53×10^{-2}	0.80	1.06	0.87
2.	$Ce_{0.90}Sr_{0.1}O_{1.90}$	1.33×10^{-3}	8.38×10^{-3}	0.83	1.01	0.97
3.	$Ce_{0.85}Sr_{0.15}O_{1.85}$	9.41×10^{-4}	5.23×10^{-3}	0.86	0.98	0.96
4.	$Ce_{0.80}Sr_{0.2}O_{1.80}$	7.34×10^{-4}	3.11×10^{-3}	0.77	0.90	0.88

[a] Data obtain from extrapolation.

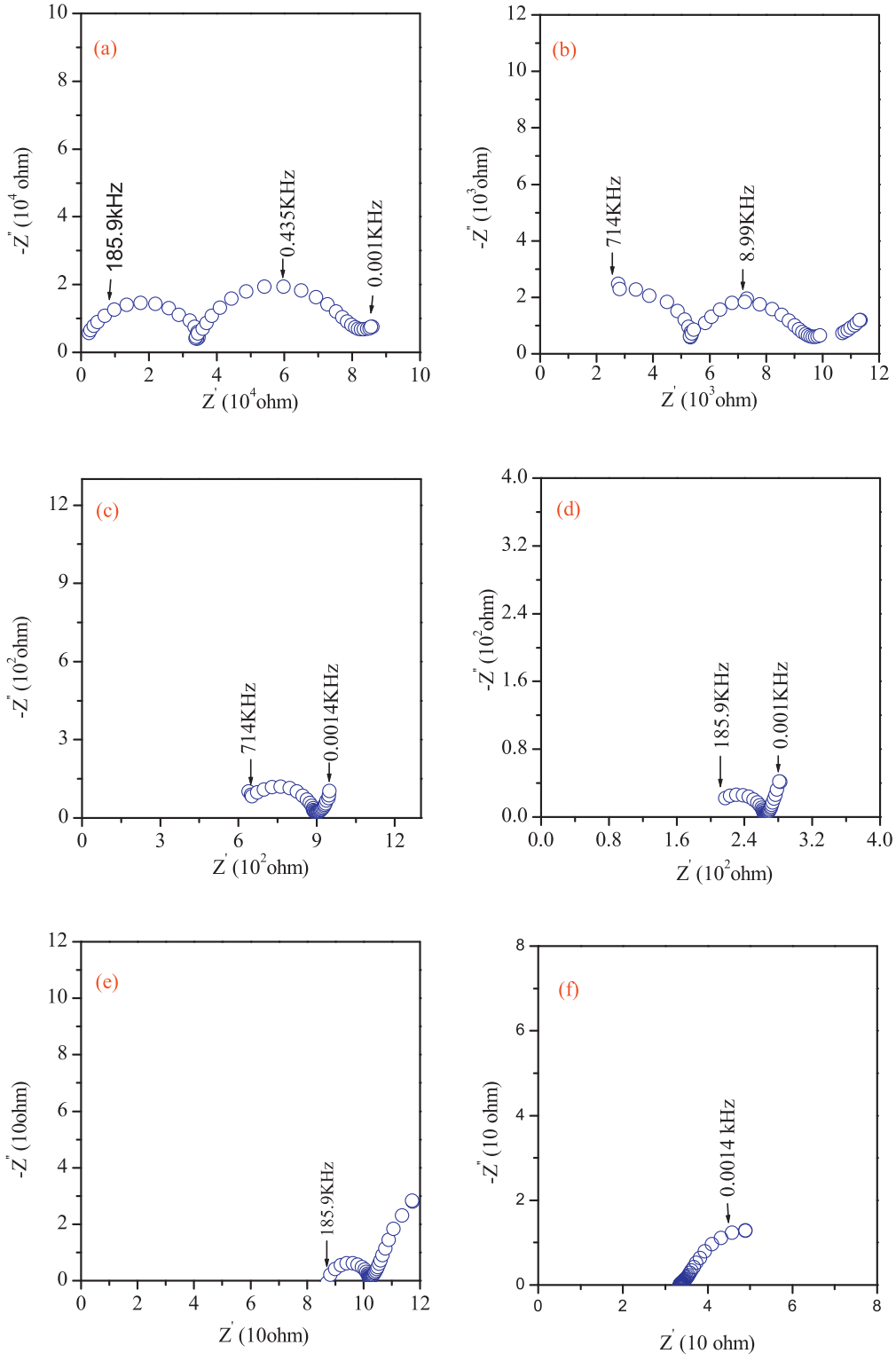

Fig. 4. Impedance plots for the composition CSO5 at (a) 200 °C, (b) 250 °C, (c) 325 °C, (d) 375 °C, (e) 425 °C and (f) 500 °C.

intercepts of these arcs with the real axis (Z'). The conductivity of grains is determined using the formula:

$$\sigma_g = \frac{L}{S \times R_g} \quad (2)$$

where σ_g is the conductivity of the grains, R_g is the resistance of the grains, L is the thickness of pellet and S is the area of the pellet. Fig. 7 shows plots of $\log \sigma_g \cdot T$ vs. $1000/T$. It shows that bulk conductivity for all the four compositions is almost equal. Conductance of the grain boundaries is maximum for CSO5 of all the four compositions and decreases in the order CSO5 > CSO10 > CSO15 > CSO20. At low temperatures, values of conductance for grain boundaries are almost equal for the last three compositions. The difference increases with increasing temperature. Since grain boundaries form a continuous path, therefore, the total conductivity σ_t vary with composition in the same manner as does G_{gb} (Fig. 9). Activation energy of

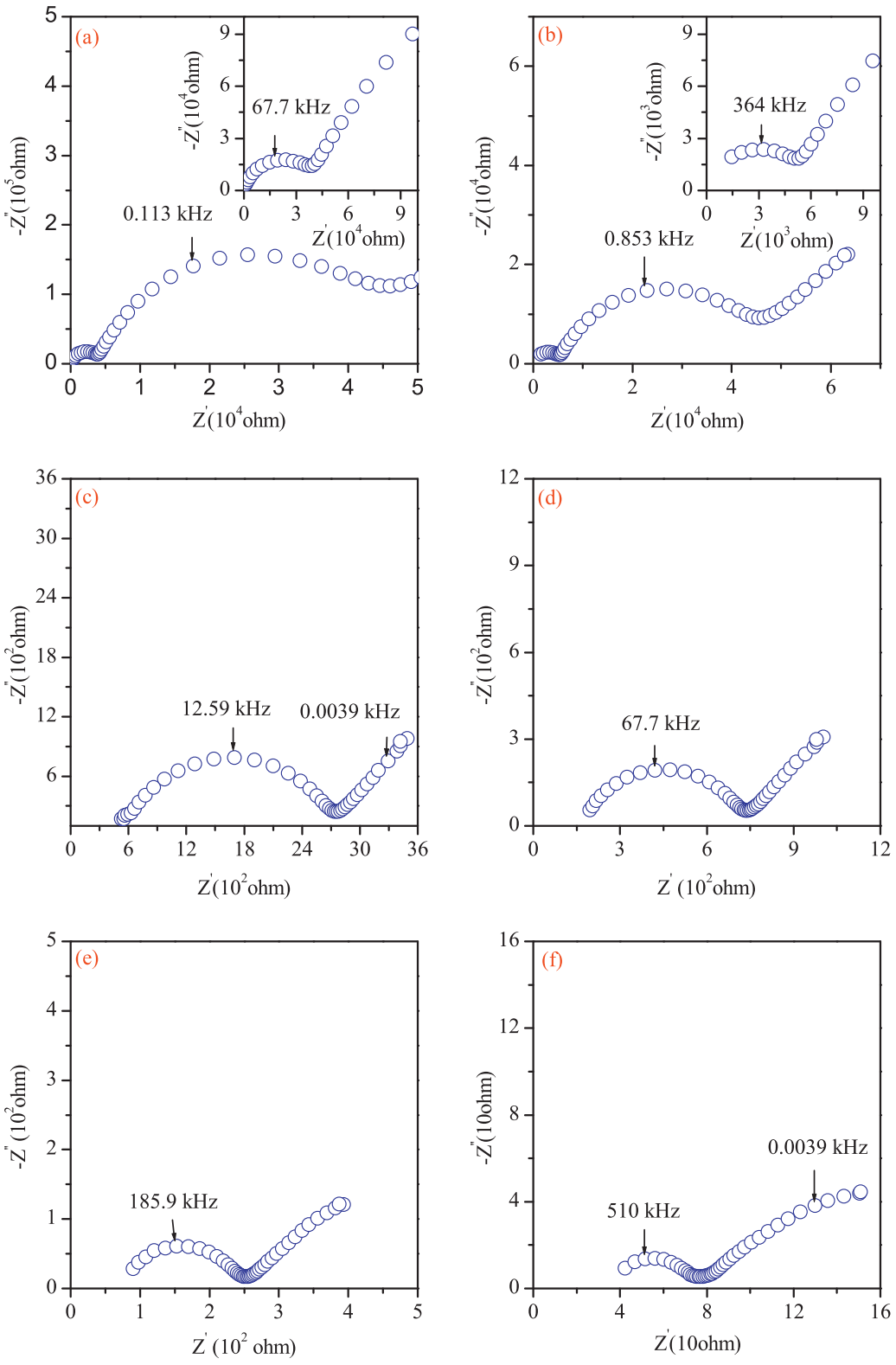

Fig. 5. Impedance plots for the composition CSO10 at (a) 200 °C, (b) 250 °C, (c) 325 °C, (d) 375 °C, (e) 425 °C and (f) 500 °C.

conduction for the grains, E_g was determined by fitting the data in Fig. 7 to Arrhenius relationship:

$$\sigma_g = \frac{\sigma_{0g}}{T} \exp\left(\frac{-E_g}{kT}\right) \quad (3)$$

where σ_{0g} is the pre exponential factor, k is the Boltzmann constant and T is the absolute temperature. Values of E_g for all the compositions determined from the plots are given in Table 2.

Fig. 8 shows $\log G_{gb} \cdot T$ vs. $1000/T$ plots for all the compositions, where G_{gb} is the conductance due to grain boundaries. These plots

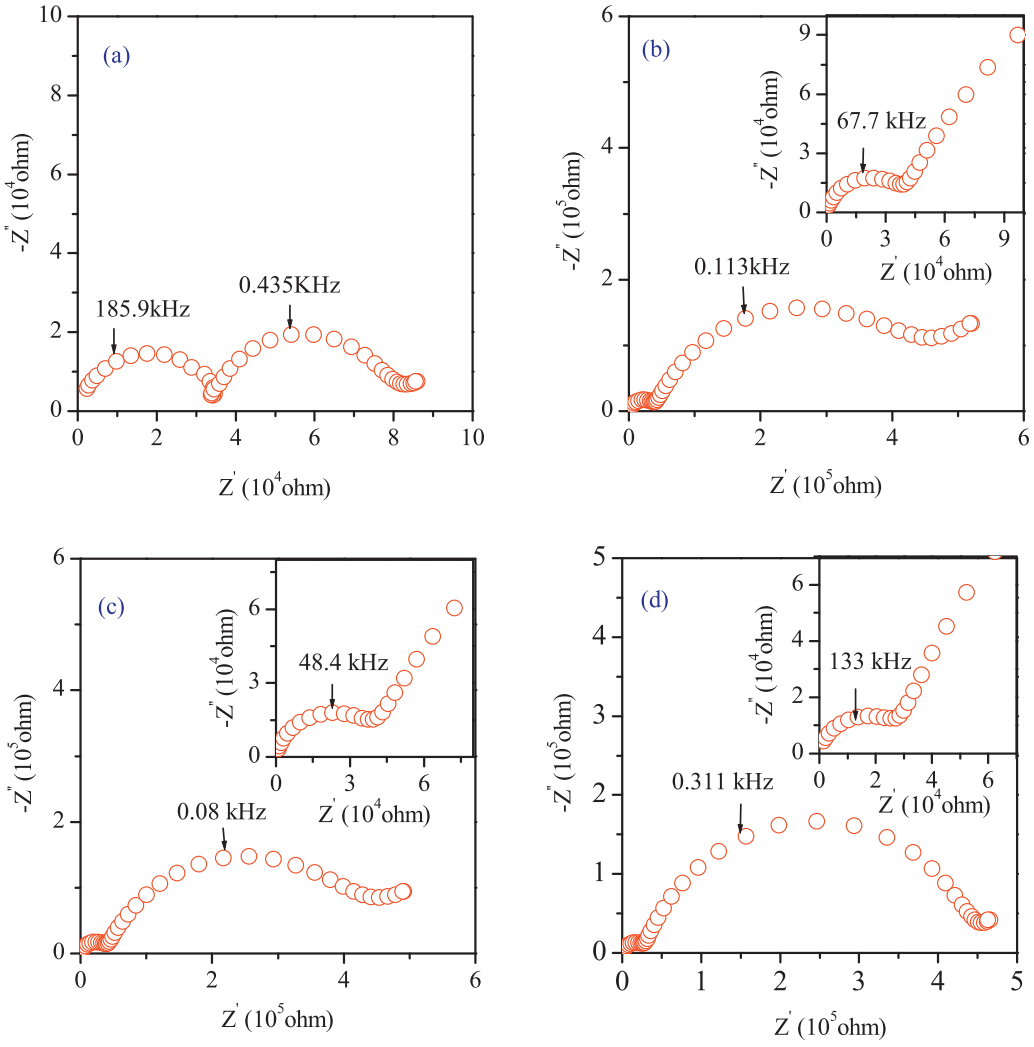

Fig. 6. Impedance plots for various compositions (a) CSO5, (b) CSO10, (c) CSO15 and (d) CSO20 at 200 °C.

are linear in the entire temperature range of measurement. CSO5 exhibits maximum value of G_{gb} of all the four samples. Activation energy of conduction for grain boundaries, E_{gb} for all the compositions has been determined from the plots by least square fitting of data points in Fig. 8 and is given in Table 2.

Total resistance of the sample is given by $R_t = R_g + R_{gb}$. Total conductivity, σ_t has been determined using the relation:

$$\sigma_t = \frac{L}{S \times R_t} \quad (4)$$

where L is the thickness and S is the area of the sample.

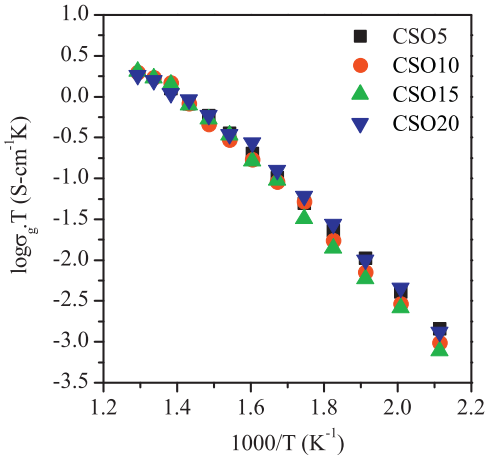

Fig. 7. $\log \sigma_g \cdot T$ vs. $1000/T$ plots of various compositions of the system $Ce_{1-x}Sr_xO_{2-x}$.

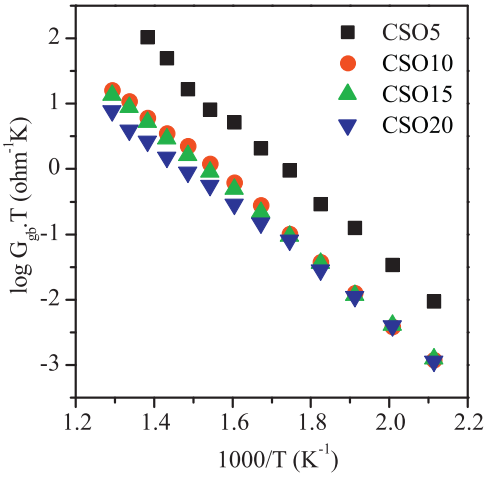

Fig. 8. $\log G_{gb} \cdot T$ vs. $1000/T$ plots of various compositions of the system $Ce_{1-x}Sr_xO_{2-x}$.

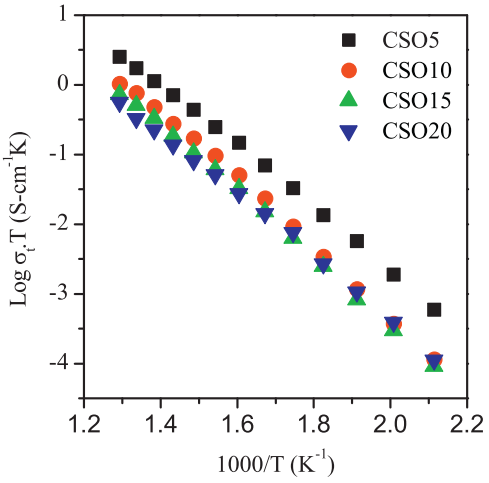

Fig. 9. $\log \sigma_t \cdot T$ vs. $1000/T$ plots of various compositions of the system $Ce_{1-x}Sr_xO_{2-x}$.

Plots of $\log \sigma_t \cdot T$ vs. $1000/T$ for all compositions are shown in Fig. 9. These plots are essentially similar to the plots of corresponding compositions in Fig. 8. This is due to fact that grain boundaries form continuous path in the sample. Therefore, total conductivity σ_t, varies in the same manner with temperature as does G_{gb}. These plots are linear with single slope in the entire temperature range of measurement. Activation energy of total conductivity, E_t for all the compositions has been determined as discussed earlier. Values of E_g, E_{gb} and E_t are given in Table 2. It is observed that values of E_{gb} and E_t are almost equal and are more than the corresponding E_g values as expected. These values of activation energy are found to agree with the reported values for the singly doped and co-doped CeO_2 in the range 0.55–1.3 eV [17]. Values of activation energies show that conduction occurs due to migration of oxygen vacancies.

Values of σ_t at 500 and 600 °C for different compositions are given in Table 2. It is noted from the table that composition with $x = 0.05$ exhibits the highest conductivity among all the compositions. Its conductivity is almost equal to the highest reported values of conductivities for compositions $Ce_{0.8}\ Sm_{0.2}\ O_{1.9}$ (1.20×10^{-2} S cm^{-1}) [9] and $Ce_{0.8}\ Gd_{0.2}\ O_{1.9}$ (1.29×10^{-2} S cm^{-1}) [10] at 600 °C. This makes it a potential candidate as a solid electrolyte for IT-SOFC being much cheaper than rare earth doped ceria. Its compatibility with other cell component, however, is necessary for its application in IT-SOFC and this needs to be checked.

Ionic conductivity of $(CeO_2)_{1-x}(SrO)_x$ decreases gradually with increasing x. This is due to the formation of $SrCeO_3$ phase [18] and also due to higher probability of formation of neutral associated pairs, $Sr'_{Ce} - V_O^{\bullet\bullet}$ with increasing x.

4. Conclusions

A few compositions in the system $Ce_{1-x}Sr_xO_{2-x}$ with $0.05 \le x \le 0.2$ have been prepared by citrate–nitrate auto-combustion method. Single phase solid solution forms in the composition with $x = 0.05$ at as low temperature as 600 °C. All compositions with $x > 0.05$ contain $SrCeO_3$ as a minor phase along with the major fluorite solid solution. 93% of theoretical density has been achieved by sintering at 1350 °C which is about 100 °C lower than the temperature reported in the literature to achieve the same density in ceria based solid electrolytes. This is due to nano size of the powder obtained after combustion. Composition with $x = 0.05$ exhibits ionic conductivity almost equal to the best reported values for $Ce_{0.8}Sm_{0.2}O_{1.9}$ and $Ce_{0.8}Gd_{0.2}O_{1.9}$ at 600 °C. This makes it a potential candidate as a solid electrolyte for ITSOFCs being much cheaper.

Acknowledgements

Thanks are due to Department of Science and Technology, New Delhi for financial support. One of the author, Nandini Jaiswal is thankful to University Grant Commission, New Delhi for fellowship.

References

[1] N.Q. Minh., J. Am. Ceram. Soc. 76 (1993) 563–588.
[2] A.S. Nowick, D.S. Par, in: G.D. Mahan, W.L. Roth (Eds.), Superionic Conductors, Plenum, New York, 1976, pp. 395–412.
[3] C.B. Choudhary, H.S. Maiti, E.C. Subbara, in: E.C. Subbarao (Ed.), Solid Electrolytes and their Applications, Plenum, New York, 1980, pp. 1–80.
[4] B.C.H. Steele, Solid State Ionics 129 (2000) 95–110.
[5] S.W. Zha, C.R. Xia, G.Y. Meng, J. Power Sources 115 (2003) 44–48.
[6] S. Kuharuangrong, J. Power Sources 171 (2007) 506–510.
[7] H. Inba, H. Tawaga, Solid State Ionics 83 (1996) 1–16.
[8] I.E.L. Stephens, J.A. Kilner, Solid State Ionics 177 (2006) 669–676.
[9] G. Bryan Balazas, S. Robert, Glass Solid State Ionics 76 (1995) 155–162.
[10] Y.-P. Fu, S.-H. Chen, J.-J. Huang, Int. J. Hydrogen Energy 35 (2010) 745–752.
[11] H. Arai, T. Kunisaki, Y. Shimizu, T. Seiyama, Solid State Ionics 20 (1986) 241–248.
[12] J.E. Garnier, R.N. Blumenthal, R.J. Panlener, R.K. Sharma, J. Phys. Chem. Solids 37 (1976) 368–378.
[13] H. Yahiro, K. Eguchi, H. Arai, Solid State Ionics 21 (1986) 37–47.
[14] R.N. Blumenthal, J.E. Garnier, Solid State Chem. 16 (1976) 21–34.
[15] T.J.B. Holland, S.A.T. Redfern, Mineral. Mag. 61 (1997) 65–77.
[16] R.D. Shannon, Acta Crystallogr. A 32 (1976) 751–767.
[17] T. Kudo, H. Obayashi, J. Electrochem. Soc. 123 (1976) 415–419.
[18] H. Yahiro, T. Ohuchi, K. Eguchi, H. Arai, J. Mater. Sci. 23 (1988) 1036–1041.